Isolated Building Blocks of Photonic Materials: High-Resolution Excited-State Photoelectron Spectroscopy of Jet-Cooled Tetramethylethylene and 1,1′-Bicyclohexylidene

R. A. Rijkenberg and W. J. Buma*

University of Amsterdam, Faculty of Science, Institute of Molecular Chemistry, Nieuwe Achtergracht 127-129, 1018 WS Amsterdam, The Netherlands

C. A. van Walree and L. W. Jenneskens

Debye Institute, Department of Physical Organic Chemistry, Utrecht University, Padualaan 8, 3584 CH Utrecht, The Netherlands

Received: December 31, 2001; In Final Form: March 19, 2002

The spectroscopy and photophysics of tetramethylethylene and 1,1′-bicyclohexylidene have been investigated using excited-state photoelectron spectroscopy in combination with multiphoton excitation. Vibronic coupling within the full manifold of the excited singlet states has been shown to play a dominant role in determining the spectroscopic properties of these compounds. Although this vibronic coupling inhibits the determination of excited state excitation energies by excitation spectroscopy, it enables at the same time their observation in the photoelectron spectra. As a result, a large number of previously unobserved Rydberg states could be located and assigned. For both molecules ionization from the Rydberg states is observed to be heavily perturbed by ionization from the underlying quasi-continuum of the (π,π*) valence state. The photoelectron spectra of 1,1′-bicyclohexylidene reveal that the state around 55000 cm^{-1} (6.82 eV), which has previously been assigned as a second valence state, does not show the ionization pattern expected on the basis of previous suggestions made for the character of this state. On the basis of this observation, configuration mixing between the (π,π*) valence state and the (π,3d) Rydberg manifold is offered as a possible explanation.

I. Introduction

Oligo(cyclohexylidenes), hydrocarbons built up from 1,4-linked cyclohexylidene units, are compounds with a $\sigma-\pi-\sigma$ orbital topology that have attracted considerable interest because of their potential application in functionalized organic materials.[1−9] In particular, photoinduced electron transfer and conductive properties are of interest in this respect. The basic unit of oligo-(cyclohexylidenes) is 1,1′-bicyclohexylidene (BCH): see Figure 1 for its molecular structure. Although the spectroscopy of this chromophore has been studied using several techniques including UV absorption, electron energy-loss (EEL) spectroscopy, and multiphoton ionization (MPI) spectroscopy,[10,11] the most striking aspect of its photophysics has not been settled yet unambiguously. The UV absorption spectrum of BCH vapor shows two broad bands of similar intensity at 48000 and 55000 cm^{-1}.[10] In an *n*-pentane solution these bands shift to 48500 and 55250 cm^{-1},[12] in a stretched polyethylene film to 48250 and 54200 cm^{-1},[13] while in a single crystal they are found at 48000 and 51000 cm^{-1}.[10] This environmental dependence was taken as evidence for their assignment as two low-lying valence excitations. From polarization studies in the solid state it was moreover shown that under these conditions the electronic transition moment associated with both excitations is directed along the C═C bond.[10]

The presence of two low-lying valence excitations is remarkable, since a priori considerations suggest only the (π,π*) state as a low-lying valence state. Several assignments have been put forward in the literature to explain the presence of two strong electronic transitions.[10,11,13−16] Although it is clear that one of the two states is the (π,π*) valence state, even its spectral location has been subject of debate. In the early work by Snyder and Clark,[10] the band at 55000 cm^{-1} was assigned to the (π,π*) valence state, an assignment that was sustained in later studies on steroids by Yogev et al.[13] and in ab initio studies by Watson et al.[15] However, the assignment of the band at 48000 cm^{-1}

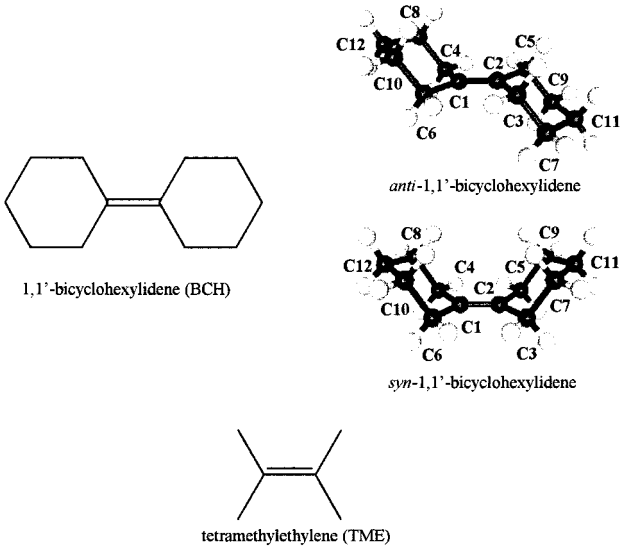

Figure 1. The molecular structures of 1,1′-bicyclohexylidene, including that of the *anti*- and *syn*-conformer of 1,1′-bicyclohexylidene, and tetramethylethylene.

* To whom correspondence should be addressed. E-mail: wybren@science.uva.nl. FAX: (31)-20-525 6456/6422

10.1021/jp014685g CCC: $22.00
Published on Web 05/03/2002

remained matter of debate. Snyder and Clark assigned it to a $\sigma \rightarrow \sigma^*$ valence transition.[10] This was supported by Yogev et al.,[13] but they also proposed an alternative assignment based upon the concept of Rydberg-valence mixing between the (π,π^*) valence state and the $(\pi,3p_y)$ Rydberg state as has been extensively advocated by Peyerimhoff et al. for ethylene.[17−19] Watson et al.[15] reached the conclusion in their theoretical studies on ethylene that the band at 48000 cm^{-1} corresponds to a vibronically induced transition to the $(\pi,3s)$ Rydberg state coupled to the (π,π^*) valence state.

An entirely different assignment for the (π,π^*) valence state was first suggested by Allan et al. in their studies on the excited states of BCH.[11] They assigned the band at 48000 cm^{-1} to the (π,π^*) valence state and tentatively suggested that the second band was due to a $\pi(CH_2) \rightarrow \pi^*$ valence transition involving charge transfer from the cyclohexyl rings into the C═C bond. Jenneskens et al.[16,20,21] corroborated in a number of ab initio studies on BCH the assignment of the lower absorption band as due to excitation of the (π,π^*) valence state, but came to an alternative assignment for the band at 55000 cm^{-1}. Their ab initio calculations indicated that this band should be assigned to a $\pi \rightarrow \sigma^*$ valence transition in which the charge transfer occurs from the C═C bond into the cyclohexyl rings. Surprisingly, it was found that this low-lying valence transition only occurs for the *anti*-conformer of BCH;[16,20,21] for the *syn*-conformer, which is present in nearly identical amounts in solution and gas phase, a differently polarized $\pi \rightarrow \sigma^*$ valence transition was calculated, being ca. 1 eV higher in excitation energy.[22] The fact that the calculated oscillator strength for the $\pi \rightarrow \sigma^*$ valence transition in the *anti*-conformer is significantly lower than that calculated for the (π,π^*) valence state, whereas the solution and gas-phase experiments—in which in this scenario the *anti*-conformer is the only one contributing to the higher energy band, while both conformers contribute to the lower one—indicates that both transitions have similar oscillator strengths, and the rather large difference between observed and calculated energy gaps remained, however, points of concern.

One would think that studies of other alkylated ethenes could lead the way to a better understanding of the spectroscopic properties of BCH. In that sense tetramethylethylene (TME)—see Figure 1 for its molecular structure—seems an ideal reference compound, but as yet no studies have reported a second valence-like absorption band in this molecule. In common with other methyl-substituted derivatives of ethylene, the gas-phase UV absorption spectrum of TME shows a strong band with its maximum at 53500 cm^{-1} (6.63 eV)[23] and weak low-energy features that start around 43100 cm^{-1} (5.34 eV).[24] Although the assignment of the intense band at 53500 cm^{-1} as the (π,π^*) valence state is generally accepted, there has been and still is a controversy as to whether the features starting at 43100 cm^{-1} are associated with the (π,π^*) valence state[25] or the $(\pi,3s)$ Rydberg state.[23−31] Previous experimental studies[32] of these features have shown that the line widths and excitation energies of these features are very sensitive to pressure, in contrast to the intense band assigned to the (π,π^*) valence state. This is exactly what is anticipated traditionally for Rydberg states because of their nature, which is more diffuse than that of valence states. This "solid state" effect on the weak features around 43100 cm^{-1} is probably the most convincing argument for their assignment as corresponding to vibronic transitions from the electronic ground state to the $(\pi,3s)$ Rydberg state.

Excited-state photoelectron spectroscopy is particularly well suited to study the vibronic properties of excited states.[33,34] The resonance-enhanced multiphoton ionization (REMPI) pump−probe scheme in combination with kinetic-energy-resolved photoelectron detection provides detailed information about the internal energy left in the ionic manifold upon ionization from an intermediate electronically excited state. If this intermediate state is primarily of Rydberg character, we generally observe that a $\Delta v=0$ propensity rule predominates, leading to a one-to-one correlation between the internal energy left within the ionic manifold and the vibrationally excited level populated in the intermediate Rydberg state. Valence states, on the other hand, generally have a different equilibrium geometry and vibrational force field than the ionic state to which ionization occurs. As a result, one expects for these states vibrational activity in the photoelectron spectrum in those vibrational modes that are associated with the change in equilibrium geometry upon ionization. Strong vibrational activity can in particular be expected for the (π,π^*) valence state of substituted ethylenes, which has a perpendicular equilibrium geometry.[17,35−39] The projection on the ionic manifold may thus serve as an excellent tool to characterize an excited state.

In the present excited-state photoelectron spectroscopic study we will focus on the spectroscopy and photophysics of TME and BCH, and try to establish the nature and origin of the second valence excitation in BCH. We will show that vibronic coupling pervades at all levels the spectroscopy and ionization dynamics of these molecules, allowing us to characterize their Rydberg manifold without performing excitation spectroscopy. Although the present study does not provide us with direct evidence for the identity and character of the second valence state in BCH, it does enable us to put forward an alternative suggestion for the origin of this state that is corroborated by other experimental and theoretical evidence.

II. Experimental Section

The results reported in this study have been obtained using a home-built magnetic bottle spectrometer equipped with a pulsed injector. Previous studies[34,40,41] have described in detail the characteristics and merits of this approach for the study of electronically excited states. We will therefore give only a brief summary of the experimental methods used here.

The laser system consists of a XeCl excimer laser (Lambda Physik EMG103MSC) working at a typical repetition rate of 30 Hz that pumps a dye laser (Lumonics HyperDye-300). The output of this dye laser can be frequency-doubled using an angle-tuned BBO or KDP crystal in an Inrad Autotracker II unit. The pulse duration of the resulting excitation beam is about 15 ns and its spectral bandwidth before frequency-doubling is about 0.07 cm^{-1}. A typical pulse energy of the fundamental laser beam leaving the dye laser is about 10 mJ which is reduced to about 1 mJ per pulse after frequency-doubling. The excitation beam is focused into the ionization region of the magnetic bottle spectrometer by a quartz lens with a focal length of 25 mm. The "2π analyzer", forming the heart of the spectrometer, is based on a design by Kruit and Read.[42] The spectrometer is equipped with a pulsed injector. Close to the injector a sample container has been installed that can be heated in order to obtain sufficient vapor pressure of the compound under investigation. Typically, the temperature of the nozzle orifice is set about 10 °C higher than the sample container in order to prevent any clogging of the injector. The maximum temperature is limited by the use of a high-temperature body coil (General Valve) suited for the pulsed operation of the molecular beam up to a temperature of about 235 °C. The laser pulse and molecular beam are synchronized by a home-built delay generator.

The magnetic bottle spectrometer can be used in either a time-of-flight (TOF) mass-resolved detection mode (TOF−MS) or

in a TOF photoelectron detection mode (TOF−PES). In the present experiments, the magnetic bottle spectrometer has been employed exclusively in the electron detection mode that has a 50% collection efficiency. This high collection efficiency is achieved by a strongly diverging magnetic field in the ionization region that parallelizes the trajectories of the produced photoelectrons. The TOF−PES technique allows for the analysis of the kinetic energies of the electrons produced in the resonance enhanced multiphoton ionization (REMPI) process via intermediate electronically excited states. The typical resolution for the TOF−PES mode is between 10 and 15 meV (80−120 cm^{-1}). After detection of the photoelectrons by a pair of microchannel plates, the signal is stored in a 500 MHz digital oscilloscope (Tektronix TDS540), which is read out by a computer. In a typical experiment, 90−150 laser pulses were averaged at each interval in both excitation as well as photoelectron scans in order to minimize the effect of pulse-to-pulse laser energy fluctuations.

The pulsed supersonic expansion is generated by a General Valve Iota One System. The expansion chamber, evacuated by an Edwards Diffstak 2000 oil pump backed by an Edwards E2M40 rotary fore pump, is connected to the ionization chamber through a skimmer (Beam Dynamics) with a diameter of 0.5 mm. The pulsed valve with an orifice of 500 μm can be set to a distance from 0 to 4.5 cm above the skimmer. The ionization chamber, located 20 cm below the skimmer, is evacuated by a Balzers TPH 170 turbomolecular pump backed by a Leybold Trivac D16B rotary fore pump. The flight tube in turn is pumped by a Leybold Turbovac 450 turbomolecular pump backed by a Leybold Trivac D25B rotary fore pump.

The pulse duration of the injector was typically set at 200 μs. At a repetition rate of 30 Hz this resulted in a pressure in the $10^{-4}-10^{-5}$ mbar range in the expansion chamber as measured with a Penning gauge (Edwards CP25−K). The pressure in the flight tube, on the other hand, does not measurably depend on the inlet of gas via the nozzle system and remains about 1×10^{-7} mbar as measured by a high-vacuum ionization gauge (Leybold IE20). In some experiments, gas was also effusively introduced into the spectrometer. In those cases the pressure in the flight tube is typically kept at a typical value of around 1×10^{-6} mbar.

The samples studied consisted of tetramethylethylene and 1,1′-bicyclohexylidene. TME, also referred to as 2,3-dimethyl-2-butene, has been commercially obtained from Fluka and used without any further purification. BCH has been synthesized by Hoogesteger using the 2-fold extrusion methodology.[12] Experiments on TME have been carried out using molecular beam expansions of TME seeded in helium. At room temperature, TME is a colorless liquid with a high vapor pressure. It is known that this high vapor pressure can lead to the formation of clusters in supersonic molecular beam expansions. For this reason some experiments on jet-cooled TME have been performed using the vapor of TME at lower temperatures of 0 and −30 °C. From these experiments, we concluded that no observable effect of clustering could be observed. The experiments performed on BCH have been carried out introducing BCH either via an effusive beam into the spectrometer or by using supersonic jet expansions of BCH seeded in helium maintaining a typical backing pressure of about 2−4 bar. To obtain sufficient BCH vapor pressure, BCH was heated to a temperature of about 70 °C, well above its melting point of 55.6 °C.[12] However, the use of molecular beam expansions did not always prove to be necessary and in order to get more ionization signal and a better signal-to-noise ratio, BCH was also effusively introduced into the spectrometer. This did not require any heating, since enough vapor pressure could already be obtained by sublimation of the BCH crystals by evacuating directly the container holding the sample using the high-vacuum system of the spectrometer itself.

III. Results and Discussion

Since in the present excited-state photoelectron spectroscopic study the (ro)vibronic wave function of an intermediate (ro)vibronically excited state is projected onto the ground state of the lowest radical cation D_0, it is essential to know the characteristics of its potential energy surface, i.e., the equilibrium geometry and its force field. Moreover, it stands to reason that the potential energy surface of the Rydberg states of both TME and BCH will to a large extend mimic that of D_0. Investigation of the spectroscopic characteristics of D_0 of both TME and BCH may therefore provide us with valuable insights into the spectroscopic and dynamical properties of the Rydberg manifold. For this reason we will first be concerned with the results of ab initio calculations we performed on the properties and characteristics of the ground state of the lowest radical cation of both TME and BCH (section A).

In the subsequent two Sections, we will report and discuss the results of our excited-state photoelectron spectroscopic studies on TME (section B) and BCH (section C). Experimental evidence will be presented that shows a strong and dominant interaction between the Rydberg manifold and the underlying continuum of the valence state(s) in both mono-olefinic compounds. This interaction results in highly complex and congested ionization patterns, but allows us at the same time to determine the spectral location of a large number of Rydberg states in both TME and BCH without recording excitation spectra.

Finally, we will discuss in section D the nature and characteristics of the valence excitations in TME and BCH. As indicated in the Introduction, one would intuitively assume that compounds such as these have only one low-lying valence state—the (π,π*) valence excitation—but the UV absorption spectrum of BCH in gas, liquid, and solid states shows two bands that have been attributed to the presence of two valence states. On the basis of the multiphoton ionization behavior of BCH as reflected in the photoelectron spectra, we will discuss the characteristics and the possible nature of this second excitation in BCH. Moreover, we will show that previous experimental studies on other mono-olefins also provide evidence for a second low-lying excitation with considerable oscillator strength in these compounds.

A. The Ground State of the Radical Cation of Tetramethylethylene and 1,1′-Bicyclohexylidene. For ethylene it is by now well-established that the equilibrium geometry of the Rydberg states and the ground state of the radical cation D_0 is significantly twisted around the C═C bond.[39,43−46] Simulation of the features of the He(I) photoelectron spectrum of the $D_0(1^2B_{3u}) \leftarrow S_0(1^1A_g)$ transition in ethylene has indicated a torsional angle of about 25° in D_0.[43−45] Simple ab initio techniques such as UHF fail to reproduce this twisted structure; extensive configuration interaction as used by Buenker et al.[46] is needed to predict the twisted structure. The experimental and calculated energy difference between the planar[44] and twisted[43] structure is 270 ± 150 and 234 cm^{-1}, respectively. A recent UB3LYP/6-311G* calculation[34] on the ionic ground state of ethylene has reproduced these features very well: it leads to a twisted structure with a torsional angle of about 27° that is stabilized with respect to the planar structure by about 235 cm^{-1}. Encouraged by the results of these calculations, we have used a similar approach to investigate the ground state of the radical cation of TME and BCH.

TABLE 1: Geometrical Parameters (Ångstroms and Degrees) and Energy (Hartrees) of the Equilibrium Geometry for the $S_0(1^1A_g)$ Ground State of Neutral Tetramethylethylene and the $D_0(1^2B_{3U})$ Ground State of the Radical Cation Calculated at the (U)B3LYP/6-31G* Level[a]

	$S_0(1^1A_g)$ B3LYP/6-31G*	$D_0(1^2B_{3u})$ B3LYP/6-31G*	
parameter	planar	planar	twisted
r(C═C)	1.349	1.436	1.432
r(C−CH_3)	1.514	1.486	1.487
∠(H_3C−C−CH_3)	111.2	117.3	117.4
∠(C═C−CH_3)	124.4	121.3	121.3
τ (H_3C−C═C−CH_3)	0.0	0.0	11.7
energy	−235.856 695	−235.569 619	−235.570 226

The ground state of the radical cation of both mono-olefinic compounds arises from the removal of an electron from the highest occupied π-orbital. In the case of TME with a molecular geometry of D_{2h} symmetry, this leads to a $^2B_{3u}$ ionic state. For BCH this line of argument is less straightforward since BCH has two conformers, i.e., *syn* and *anti*, that possess C_{2v} and C_{2h} symmetry, respectively. The molecular structure of both conformers is drawn in Figure 1. Removal of an electron from the highest occupied π-orbital of the *syn*- and *anti*-conformer results in a state of $^2A_1$ and ^2B_u symmetry, respectively. In the solid state, the symmetry of BCH is lowered to C_i,[47] though it is still very close to C_{2h}. However, ^{1}H NMR spectroscopy of BCH dissolved in chloroform at 300 K[45,48] has shown convincingly that rapid ring interconversions between both conformers occur since no distinct resonances of equatorial and axial hydrogen atoms of the cyclohexyl rings can be observed. Previous ab initio calculations[22] have indicated that both structures have nearly the same total energy. They predict that the *syn*-conformer is slightly more stable than the *anti*-conformer by about 0.051 kcal/mol, suggesting an equilibrium mixture consisting of 52% *syn*- and 48% *anti*-conformer at 300 K. These observations lead to the conclusion that also in the gas phase a nearly 1:1 ratio of the two conformers can be expected.

Similar to ethylene,[34] UB3LYP/6-31G* geometry optimization of the ground state of the radical cation of TME and BCH leads to slightly twisted structures. For TME a geometry is calculated that is twisted with a torsional angle of about 11° around the central C═C bond, and has an energy that is a mere 133 cm^{-1} below the planar structure. The relevant geometrical parameters of both structures are reported in Table 1. For comparison, also the parameters calculated at the B3LYP/6-31G* level for the neutral ground state are included in this table. Both structure and energy of the ionic ground state are in perfect agreement with a previous UHF/3-21G ab initio study on methyl-substituted ethylenic radical cations where a dihedral angle of about 11° and a barrier of about 140 cm^{-1} were predicted.[49] Although twisting around the C═C bond lowers the symmetry of the molecule from D_{2h} to D_2, tunneling through the low energy barrier leads to a dynamic symmetry that is still D_{2h}. The same kind of observations have been made for the ground state of the radical cation of ethylene and its Rydberg manifold.[34,44,45,50−52] Moreover, analogous to the situation in ethylene,[34,44,45,50] the double-well potential of the ground state of the lowest radical cation of TME may be expected to lead to a very strong anharmonicity with respect to the C═C torsional mode.

The harmonic force field calculated for D_0 at the twisted equilibrium geometry gives rise to the vibrational frequencies reported in Table 2. Experimental data on the vibrational frequencies of D_0 are scarce. In a He(I) photoelectron study on tetra-substituted olefins a value of 1430 ± 50 cm^{-1} was reported for the frequency of the C═C stretching mode.[53] This value is in good agreement with the value calculated in the present study (1500 cm^{-1} after scaling with a factor of 0.9614).[54,55] Experimental studies using IR and Raman spectroscopy[56−58] and previous theoretical analyses of the harmonic force field of the neutral ground state of TME[59,60] have yielded a partial list of the vibrational frequencies of the molecule in S_0. The experimental values reported in Table 2 are in general in good agreement with the values calculated here at the B3LYP/6-31G* level, although the values calculated for the low-frequency CH_3 torsional modes seem to be consistently too low compared to the experimental values.[56]

It is expected that the dominant geometry changes upon ionization, and similarly upon excitation to Rydberg states, occur at the double bond, and thus that the vibrational modes that are active in ethylene are also active in TME. From this point of view, the important modes are the ethylenic totally symmetric ν_2 C═C stretching and ν_3 CH_2 scissors modes, as well as the nontotally symmetric ν_4 C═C torsional mode. Visual inspection shows that these modes can be well correlated with the totally symmetric ν_3 C═C stretching and ν_8 skeletal bending modes, and the ν_{12} C═C torsional mode of a_u symmetry, respectively, in TME. Both for S_0 and D_0 the vibrational frequencies of the $\nu_8(a_g)$ skeletal bending and the $\nu_{12}(a_u)$ C═C torsional modes in TME are significantly lower compared to their values in ethylene.[34] Focusing on D_0, the ν_8 skeletal bending mode is lowered from 1264 to 413 cm^{-1} (experimental values),[44] while the frequency of ν_{12} is reduced from 551 to 93 cm^{-1} (calculated values).[34] Interestingly, it is found that a reversal of ν_{12} and ν_{13} takes place in going from the neutral ground state to the ground state of the radical cation.

Ab initio calculations at the UB3LYP/6-31G* level on the planar and twisted geometry of the ground state of the radical cation of both *syn*- and *anti*-BCH lead to geometrical parameters reported in Table 3 (see Figure 1 for carbon labels). The dihedral angle for the twisted structures is about 20−25°. The energy difference between the planar and twisted structures is calculated as 66 and 163 cm^{-1} for the *syn*- and *anti*-conformer, respectively, which is of the same order as found for TME. Once again we may expect that as the result of tunneling the static symmetry of C_2 of both conformers turns into a dynamic C_{2v} and C_{2h} symmetry for the *syn*- and *anti*-conformers, respectively, and that the C═C torsional mode exhibits a strong anharmonicity. The present calculations and studies of *tert*-butyl end-capped bicyclohexylidenes[61] also indicate that the ionization energies of both conformers can be expected to be quite similar. Previously reported He(I) photoelectron spectra[11] indeed did not show indications for a resolvable difference between the two conformers, and this is confirmed in the present study. Concurrently, we may therefore expect that the Rydberg states of the two conformers have rather similar excitation energies.

An ab initio force field calculation at the UB3LYP/6-31G* level of the twisted equilibrium geometry of both the *syn*- and *anti*-conformer of BCH provides the vibrational frequencies associated with the 90 normal mode coordinates. This calculation shows that the totally symmetric ν_2 C═C stretching mode and nontotally symmetric $\nu_4(a_u)$ C═C torsional modes in ethylene are readily associated with vibrational modes in BCH. The calculated (unscaled) vibrational frequencies of these modes for the ground state of the radical cation of BCH are 1549 and 63 cm^{-1} for the *syn*-conformer, respectively. For the *anti*-conformer frequencies of 1553 and 58 cm^{-1} are obtained. A He(I)

TABLE 2: Experimental and Calculated ((U)B3LYP/6-31G*) Vibrational Frequencies (cm^{-1}) of Tetramethylethylene in the $S_0(1^1A_g)$ Ground State of the Planar Neutral Molecule and the $D_0(1^2B_{3u})$ Ground State of the Twisted Radical Cation

	vibration[a]	S_0 exptl	S_0 calcd[b]	D_0 calcd[b]		vibration[a]	S_0 exptl	S_0 calcd[b]	D_0 calcd[b]
a_g					b_{2g}				
1	C−H str	2920	3061	3108	25	C−H str	2920[c]	3024	2990
2	C−H str	2869	3033	2999	26	CH_3 def	1458[c]	1523	1457
3	C═C str	1676[c]	1751	1559	27	CH_3 rock	1072[c]	988	1002
4	CH_3 def	1458[c]	1502	1419	28	skel. bend	410[c]	349	305
5	CH_3 def	1394[c]	1464	1399	29	CH_3 tors	201[d]	179	103
6	CH_3 rock	1029[c]	1036	890	b_{2u}				
7	C−CH_3 str	692[c]	692	689	30	C−H str		3172	3171
8	skel. bend	413[d]	424	393	31	C−H str		3066	3110
a_u					32	CH_3 def		1534	1525
9	C−H str		3172	3170	33	CH_3 def		1446	1400
10	CH_3 def		1536	1525	34	C−CH_3 str		1167	1235
11	CH_3 rock		1069	1040	35	C═C−C wag		1110	1067
12	C═C tors	153[d]	156	93	36	C═C−C wag	417[d]	523	522
13	CH_3 tors		68	173	b_{3g}				
b_{1g}					37	C−H str		3152	3167
14	C−H str		3153	3167	38	C−H str		3066	3108
15	CH_3 def		1526	1506	39	CH_3 def		1530	1509
16	CH_3 rock		972	928	40	CH_3 def		1433	1394
17	CH_3 tors	194[d]	89	156	41	C−CH_3 st		1286	1334
b_{1u}					42	C═C−C wag		1123	1013
18	C−H str	2990[c]	3062	3107	43	C═C−C wag		346	317
19	C−H str	2860[c]	3028	2994	b_{3u}				
20	CH_3 def	1446[c]	1510	1461	44	C−H str	2915[c]	3022	2988
21	CH_3 def	1370[c]	1439	1397	45	CH_3 def	1446[c]	1507	1467
22	CH_3 rock	1167[c]	1209	1203	46	CH_3 rock	1060[c]	959	984
23	C−CH_3 str	896[c]	906	844	47	Skel. bend	311[c]	494	478
24	Skel. bend	410[c]	413	433	48	CH_3 tors	227[d]	132	67

[a] str = stretching, def = deformation, tors = torsion, skel. bend = skeletal bending, wag = out-of-plane wagging. [b] Calculated values have not been scaled. [c] Values obtained from ref 59. [d] Values obtained from ref 56.

TABLE 3: Geometrical Parameters (Ångstroms and Degrees) and Energy (Hartrees) of the Equilibrium Geometry for the $S_0(1^1A_g/1^1A_1)$ Ground State of the Neutral *anti-* and *syn*-Conformer of 1,1′-Bicyclohexylidene as Well as the $D_0(1^2B_{3U}/1^2A_1)$ Ground State of the Radical Cation Calculated at the (U)B3LYP/6-31G* Level

	anti-BCH (C_{2h})				*syn*-BCH (C_{2v})		
	$S_0(1^1A_g)$		$D_0(1^2B_u)$			$D_0(1^2A_1)$	
parameters[a]	exptl[b,c]	calcd	planar: C_{2h}	twisted: C_2[c]	$S_0(1^1A_1)$ calcd	planar: C_{2v}	twisted: C_2[c]
bond lengths							
C1−C2	1.339	1.351	1.431	1.425	1.351	1.433	1.423
C2−C3	1.511;1.514	1.520	1.490	1.490;1.491	1.520	1.490	1.492;1.491
C3−C7	1.529;1.531	1.544	1.573	1.572;1.572	1.544	1.572	1.569;1.570
C7−C11	1.523;1.519	1.534	1.530	1.530;1.529	1.534	1.529	1.531;1.529
angles							
C1−C2−C3	124.40;124.55	124.7	123.4	122.9;122.8	124.7	123.3	123.2;122,5
C2−C3−C7	112.27;111.88	111.6	109.3	109.1;109.1	111.5	109.6	109.2;109.3
C3−C7−C11	111.08;111.17	111.5	110.9	111.3;110.6	111.5	111.0	111.6;110.7
C7−C11−C9	110.42	111.2	111.9	111.8	111.2	111.6	111.7
dihedral angles							
C4−C1−C2−C3	180.0	180.0	180	161.4	179.0	180	153.8;161.7
C4−C1−C2−C5	0.7	1.8	0	12.4;24.8	0.0	0	22.3
energy		−469.328 533	−469.053 379	−469.054 715	−469.328 537	−469.053 167	−469.054 320

[a] The carbon labels are according to the molecular structures depicted in Figure 1. [b] Experimental values are single-crystal X-ray data (molecular structure of 1,1′-bicyclohexylidene has C_i symmetry in the solid state) taken from ref 47. [c] Because of relatively low symmetry (C_i for the experimentally determined neutral structure in the electronic ground state and C_2 for the calculated twisted structures of the radical cation) two entries are given for inequivalent values of geometrical parameters.

photoelectron spectroscopic study on BCH[11] exhibits a 1360 cm^{-1} progression in the ionic manifold of the *anti*-conformer, which was assigned to the C═C stretching mode. The calculated value seems to be somewhat low with respect to this value, although we notice that the calculated value for S_0—1660 cm^{-1} (scaled by 0.9614)[54,55]—is in excellent agreement with the experimentally observed IR value[59] of 1676 cm^{-1}. A more likely explanation for the observed difference is therefore that the apparent 1360 cm^{-1} progression results from the unresolved activity of more than one mode, similar to what is observed, for example, in absorption spectra of longer polyenes. The ν_3 CH_2 scissors mode of ethylene is not one-on-one identifiable in the normal modes of BCH.

B. Rydberg Excitations in Tetramethylethylene. Figure 2 shows the (1+1) REMPI excitation spectrum of jet-cooled TME in the spectral region of 41500−44000 cm^{-1} (5−5.5 eV). It shows a strong resemblance to the laser induced fluorescence (LIF) excitation spectrum of jet-cooled TME as obtained

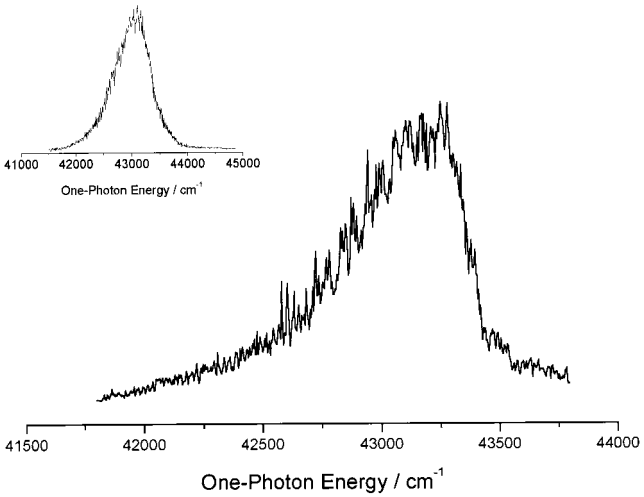

Figure 2. (1+1) REMPI excitation spectrum of jet-cooled tetramethylethylene in the one-photon energy range of 41500−44000 cm^{-1} with a helium backing pressure of 10 bar. To illustrate the importance of very efficient cooling, a similar spectrum, recorded with a backing pressure of 3 bar, is shown in the inset.

previously,[25] albeit that the current REMPI spectrum appears to be better vibrationally resolved. This particular spectrum has been recorded using a helium backing pressure of 10 bar. To show the importance of very efficient cooling, a similar spectrum, recorded with a backing pressure of about 3 bar of helium, is shown in the inset of Figure 2. Comparison of the two spectra shows that the excitation spectrum is very sensitive to cooling parameters, and that only very efficient cooling allows for partially resolved vibrational features. Although Hirayama and Lipsky[26] were the first to report the observation of fluorescence emission from TME excited at 184.9 nm, Siebrand et al.[25] were the first to significantly improve previously obtained vibrationally unresolved LIF excitation spectra of TME in the gas phase[24] and the liquid phase.[27] Their partially vibrationally resolved excitation spectrum of TME under isolated conditions allowed them to investigate the vibrational features of the highly congested excitation spectrum. Convinced of a close similarity of this spectrum with that of the $^1B_{1u}(\pi,\pi^*) \leftarrow 1^1A_g$ spectrum of C_2D_4,[62] they tentatively assigned part of the vibrational features in terms of the ν_4 torsional mode and the ν_7 CH_2 wagging mode of deuterated ethylene—of course taking differences in effective masses and bond lengths into account. They report anharmonic values for these two modes in TME of about 120 and 386 cm^{-1}, respectively. In their view, the enormous spectral congestion results from a strong anharmonicity due to excitation of TME to levels close to the top of the (π,π^*) valence state torsional barrier.

The present photoelectron spectra recorded over the 41500−44000 cm^{-1} spectral range prompt a different interpretation. As a typical example, Figure 3 shows a photoelectron spectrum recorded at 42842 cm^{-1}. Its characteristics are a dominant, broad peak at 2.332 eV with a line width of about 80 meV. Taking into account that the adiabatic ionization potential (IP) of TME is 8.271 eV[63] we conclude that the intense feature corresponds to ionization to an ionic vibrational level 169 cm^{-1} above the vibrationless level of D_0. This, in turn, implies that the vibrationless level of the state that is excited is around 42673 cm^{-1}. Given the experimental resolution of about 10−15 meV (80−120 cm^{-1}), this value is close to the peak position of the first well-resolved feature in the excitation spectrum at 42580 cm^{-1}.

The observation that ionization dominantly occurs to a specific level in the ionic manifold strongly suggests that this

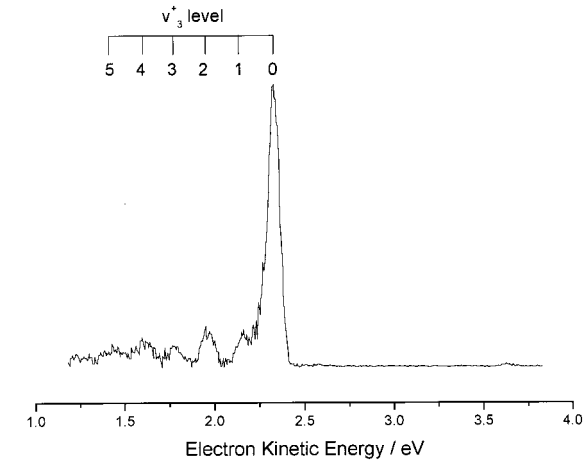

Figure 3. (1+1) REMPI photoelectron spectrum of tetramethylethylene excited at 42842 cm^{-1}.

peak in the photoelectron spectrum is associated with ionization from a Rydberg state. From the Rydberg formula we calculate $(n-\delta)=2.13$, leading to a principal quantum number n of 3 and a quantum defect δ of about 0.87. Within the D_{2h} point group this implies that this Rydberg state should be assigned as $^1B_{3u}(\pi,3s)$. The quantum defect is in perfect agreement with that reported in an absorption study of the Rydberg progressions in *cis*- and *trans*-2-butene by McDiarmid,[64] claiming a quantum defect δ of 0.87 for the $(\pi,3s)$ Rydberg state in *trans*-2-butene.

The spectral line width of the dominant feature in the photoelectron spectrum of Figure 3 is 80 meV, which is well above the resolution of about 10−15 meV that we reach under similar circumstances for ionization of noble gas atoms. We attribute the spectral broadness of this feature to the strong anharmonicity in D_0 anticipated for the Franck−Condon active low-frequency ν_{12} C═C torsional mode in TME (vide supra). Ionization from the intermediate state will then lead to unresolved ionization to the various anharmonic levels of ν_{12}, and thus to an apparent broadening of the photoelectron peak.

There are two observations in the photoelectron spectrum that imply that this is not the complete story. First, a vibrational progression with an energy spacing of 1445 cm^{-1} is observed. This energy spacing is in excellent agreement with the previously reported value of 1430 ± 50 cm^{-1} for the frequency of the C═C stretching mode in the ground state of the radical cation of TME.[53] The intensity distribution over the various members of the progression—in particular with respect to the intensity of the dominant photoelectron peak—implies, however, that they are associated with ionization from a state that is different from the one that is responsible for the dominant peak. Second, the observation that at higher photoelectron energies than the dominant peak a flat baseline is obtained, demonstrates that the "noise" that is present on and between the photoelectron peaks at lower energies actually reflects ionization to a plethora of ionic levels. This behavior is consistent with an ionization process in which the molecular geometry in the initial and final states are vastly different, and we consequently conclude that the photoelectron spectra do not only show ionization from a Rydberg state, but from the (π,π^*) valence state as well.

Previously, the vibrational features observed in the excitation spectrum have been assigned in terms of excitation of vibrational levels of the valence state.[25] Our photoelectron studies imply, on the other hand, that an explanation in terms of excitation of vibrational levels of the $(\pi,3s)$ state might also be possible. As was noticed in this previous work, the excitation spectrum consists of several groups of features that contain approximately

TABLE 4: Observed (Ethylene) and Estimated (Tetramethylethylene) Anharmonic Torsional Energy Levels (cm^{-1}) of the C═C Torsion Vibrational Mode in the $D_0(1^2B_{3u})$ Ground State of the Radical Cation of Ethylene and Tetramethylethylene

	$D_0(1^2B_{3u})$		
vibrational level C═C torsion	ethylene[a] energy	tetramethylethylene energy	tetramethylethylene spacing
0	0	0	
1	101	17	17
2	438	74	57
3	769	130	56
4	1158	195	65

[a] Experimental values have been taken from ref 44.

4 to 5 resonances grouped closely together with an average spacing of about 15 ± 5 cm^{-1}. The average spacing between these groups is about 60 cm^{-1}. On the basis of the previous experimental work on the spectroscopy of the (π,3s) Rydberg state of ethylene,[34,50−52] the spectrum of TME is expected to be dominated by excitation to anharmonic levels associated with the ν_{12} C═C torsional mode. Chau et al.[65] have calculated the four lowest anharmonic levels of the ν_4 torsional mode in both the (π,3s) Rydberg state and the lowest radical cation of ethylene. These values proved to be in excellent agreement with the experimental values.[44,45] The unscaled vibrational frequencies of the C═C torsional mode of the radical cations of ethylene[34] and TME as calculated by UB3LYP calculations are 551 and 93 cm^{-1}, respectively. Using these values and assuming a similar anharmonicity in the radical cation of TME as in $C_2H_4^+$, we can estimate the vibrational energies of the four lowest anharmonic levels in the ground ionic state of TME. These results, together with the corresponding levels in ethylene, are reported in Table 4. For the Rydberg states, in analogy to the case of ethylene, the vibrational energies are expected to be very similar. Table 4 demonstrates that the energy spacing between the ν_{12} C═C torsional levels is around 60 cm^{-1}, which is in perfect agreement with the value observed in the present excitation spectrum. We notice that this assignment implies that excitation from $S_0(1^1A_g)$ to ν_{12} levels of the $1^1B_{3u}(\pi,3s)$ Rydberg state of both even and odd parity is observed. This seems to be in contradiction to the selection rules as dictated by the D_{2h} point group, but the presence of the four methyl groups in TME may well reduce the symmetry of the molecule. In fact, the methyl groups could well be associated with the observed fine splitting of about 15 ± 5 cm^{-1} in the excitation spectrum since the hindered internal rotation of these groups can lead to "tunnelling splitting" of vibrational lines corresponding to normal modes other than CH_3 torsional movement. Similar observations have been reported for other methylated compounds such as methylated stilbenes.[66−69]

On the basis of the assignment of nontotally symmetric vibrational activity in the absorption spectra of other monoolefins,[31,64] as well as on considerations of observed and calculated oscillator strengths, it has previously been suggested that the (π,3s) transition in these compounds is partly vibronically induced via coupling to the (π,π^*) valence state.[15,30,31,64] Unfortunately, the present (1+1) excitation spectrum of the (π,3s) does not allow such a detailed vibrational analysis that would be able to corroborate such a suggestion also for TME.

The sudden drop in both ionization and fluorescence signal[25−27,29] beyond an excitation energy of 43280 cm^{-1} is a spectroscopic reflection of the dynamical properties of the excited-state photophysics of TME. Lifetimes within the ns time regime have been reported below this excitation energy;[25,29]

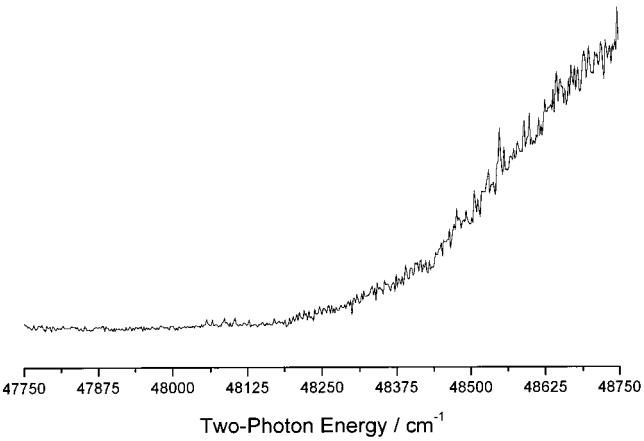

Figure 4. (2+1) REMPI excitation spectrum of jet-cooled tetramethylethylene in the two-photon energy range of 47750−48750 cm^{-1}.

above this value, they drop rapidly to the picosecond time regime.[26] In the past rapid internal conversion between the excited-state potentials of the (π,3s) Rydberg and (π,π^*) valence state has been put forward as an explanation for this relaxation channel.[26] The present results imply in that case that the vibrationless level of the (π,3s) Rydberg state is located about 700 cm^{-1} below the crossing point of these two excited-state potentials.

Although the (1+1) ionization signal rapidly decreases beyond a one-photon energy of 43280 cm^{-1}, a very weak, nonresonant ionization signal remains. For probing the electronic structure at higher excitation energies, two-photon excitation has been employed, which leads to the excitation spectrum depicted in Figure 4 for the excitation range from 47750 to 48750 cm^{-1}. This Figure shows a small, but nonzero signal that starts to increase around 48250 cm^{-1}, after which there is a continuous signal. A number of states can be expected to contribute to the ionization signal in this region. First, the $1^1B_{1u}(\pi,\pi^*)$ valence state, but because two-photon excitation is employed, a contribution from this state would need to involve vibronically induced transitions. The same would apply to contributions from the $1^1B_{3u}(\pi,3s)$ state. With respect to this state, we should also bear in mind that a dominant $\Delta\upsilon=0$ propensity for ionization is expected. For (2+1) ionization this leads to the conclusion that a (π,3s) contribution to the ionization only becomes efficient above two-photon excitation energies of 48260 cm^{-1}, which might be a possible explanation for the increase of the signal around 48250 cm^{-1}. Finally, the $^1B_{2g}(\pi,3p_z)$ Rydberg state, for which the origin has recently been reported in a magnetic circular dichroism (MCD) study[14] at room temperature to be around 48900 cm^{-1}, may be expected in this energy region.

Ionization in this region is observed to involve three channels. Figure 5 shows as a typical example the photoelectron spectrum recorded at a two-photon energy of 48750 cm^{-1}. It is dominated by two relatively intense features at nearly zero kinetic energy (0.064 eV) and at 0.795 eV. The latter value can be associated with ionization to the vibrationless level of D_0, which in turn—on the basis of a $\Delta\upsilon=0$ propensity—implies that ionization has occurred from an excited vibrationless level. This is in good agreement with the experimentally reported MCD value of the origin region of the ($\pi,3p_z$) Rydberg state.[14] The zero-kinetic energy feature cannot be attributed to ionization from this ($\pi,3p_z$) Rydberg state since this would imply that ionization would occur to an ionic vibrational level with 5904 cm^{-1} vibrational energy. However, the energy difference of 731 meV between the two intense features in the photoelectron spectrum corresponds, given

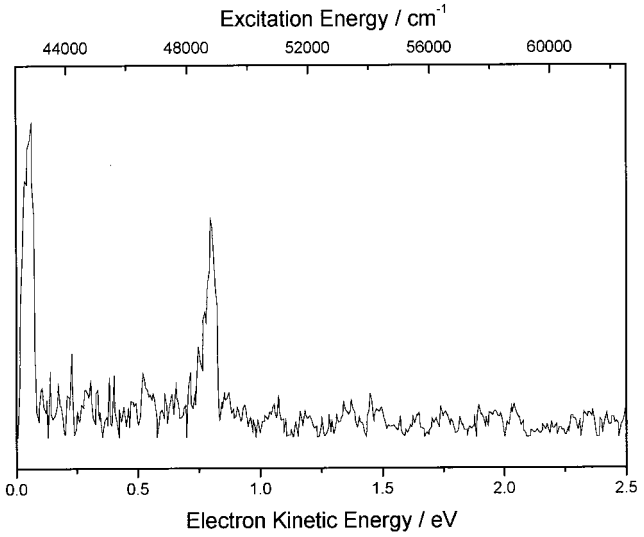

Figure 5. (2+1) REMPI photoelectron spectrum of tetramethylethylene excited at 48750 cm^{-1}.

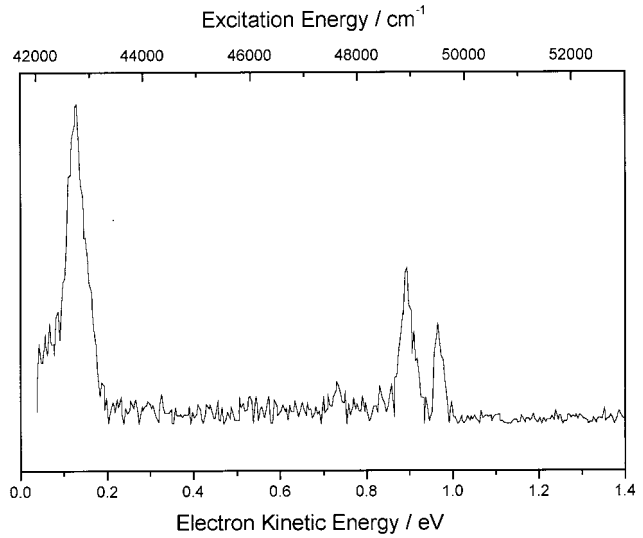

Figure 6. (2+1) REMPI photoelectron spectrum of tetramethylethylene excited at 50000 cm^{-1}.

the width of the photoelectron peaks, to a good extent with the energy difference of 765 meV between the vibrationless levels of the (π,3s) and (π,3p_z) Rydberg states. The feature at 0.064 eV can therefore be readily assigned to ionization from the (π,3s) Rydberg state. If one assumes a $\Delta v=0$ ionization in which the vibrational energy is more or less conserved, one can thus associate with each photoelectron energy an excitation energy of an intermediate state. This scale is the second *x*-axis drawn on top of the figure.

Furthermore, the photoelectron spectrum in Figure 5 shows not only one-photon ionization from the (π,3p_z) and the (π,3s) Rydberg states but also features exceeding the maximum electron kinetic energy of 0.795 eV available for a (2+1) ionization process. These features are attributed to (2+2) photoionization. Without a retarding voltage in the flight tube these features all coincide in the time-of-flight spectrum and lead to a peak of considerable intensity that may even be larger than the photoelectron peaks associated with ionization of the (π,3p_z) and the (π,3s) Rydberg states. Recording the photoelectron spectrum by increased retardation of the photoelectrons, as we normally do, is observed to be similar to the peeling of an onion, and leads to the many features of low intensity visible in Figure 5. Such a spectrum is typical for photoionization from a state with an equilibrium geometry that is very different from that of the lowest radical cation, and suggests ionization from the (π,π*) valence state.

Considering two-photon selection rules and the Franck−Condon factors for excitation of the various states, it is most likely that we observe around 48250 cm^{-1} the resonance enhanced two-photon excitation from S_0 to the origin region of the $^1B_{2g}$(π,3p_z) Rydberg state. At the same time, our observations indicate that vibronic coupling, or internal conversion in a time-domain picture, plays a dominant role in the photophysics of TME at these excitation energies. As a result, not only ionization of the $^1B_{2g}$(π,3p_z) Rydberg state is observed, but also ionization of high-lying vibronic levels of the $^1B_{3u}$(π,3s) Rydberg state and the $^1B_{1u}$(π,π*) valence state. This conclusion is reinforced by photoelectron spectra obtained at higher excitation energies of up to 49300 cm^{-1} that show a similar pattern as seen in Figure 5. At higher excitation energies, an additional peak comes into the photoelectron spectra. As an example, the photoelectron spectrum obtained after two-photon excitation at 50000 cm^{-1} is depicted in Figure 6. This additional peak can be associated with $\Delta v=0$ ionization from a state at 49300 cm^{-1}, which, because of its quantum defect, suggests a (π,3p) Rydberg state.

At this stage it is clear that the study of the spectroscopy of the lower Rydberg states in TME using excited-state photoelectron spectroscopy leads to a complex and congested ionization pattern. Moreover, although excited-state photoelectron spectroscopy allows us to monitor selectively the kinetic energies of photoelectrons associated with the ionization of a specific intermediate Rydberg state, the excitation profile is completely obscured by the couplings between the valence and Rydberg manifold. This internal conversion creates a constant population in the vibrational manifold of the Rydberg states, and leads to a constant ionization signal from those Rydberg states that are accessible at a certain excitation energy. The only exception is the lowest $^1B_{3u}$(π,3s) Rydberg state, which shows a clear, but highly congested, excitation profile. However, the excitation profile of the (π,3p) Rydberg manifold is lost, and no resonant features can be seen.

The above observations suggest that we can actually employ the interstate couplings to determine excitation energies of higher Rydberg states without taking excitation spectra. To this purpose, we have recorded several photoelectron spectra using (3+1) and (2+1) ionization schemes in the excitation region from 52000 cm^{-1} to the IP of TME. Both two- and three-photon excitation schemes lead to similar photoelectron spectra. Figure 7 shows two photoelectron spectra recorded at a three-photon energy of 57000 (7.067 eV) and 65500 cm^{-1} (8.121 eV), the latter value being quite close to the adiabatic IP of TME (8.271 eV).[63] At 57000 cm^{-1} a photoelectron spectrum is obtained with three dominant peaks located at 0.127, 0.741, and 0.860 eV. These signals correspond to one-photon ionization from intermediate electronically excited levels located at 48734, 53686, and 54646 cm^{-1}, respectively. The 48734 cm^{-1} level has been assigned in the (2+1) ionization experiments described above to the $^1B_{2g}$(π,3p_z) Rydberg state. The other two levels at 53686 and 54646 cm^{-1} are assigned to the (π,3d) and (π,4s) Rydberg states, respectively. Quantum defects of 0.10 and 0.98 are calculated from these excitation energies, respectively, which agree well with the quantum defects reported for (π,*n*d) and (π,*n*s) Rydberg states for *trans*-2-butene.[64] A fourth, rather weak, ionization signal is observed at 0.196 eV. This signal agrees well with what is expected for ionization from the ^1A_g(π,3p_x) Rydberg state at 49291 cm^{-1}. Ionization from the $^1B_{3u}$(π,3s) Rydberg

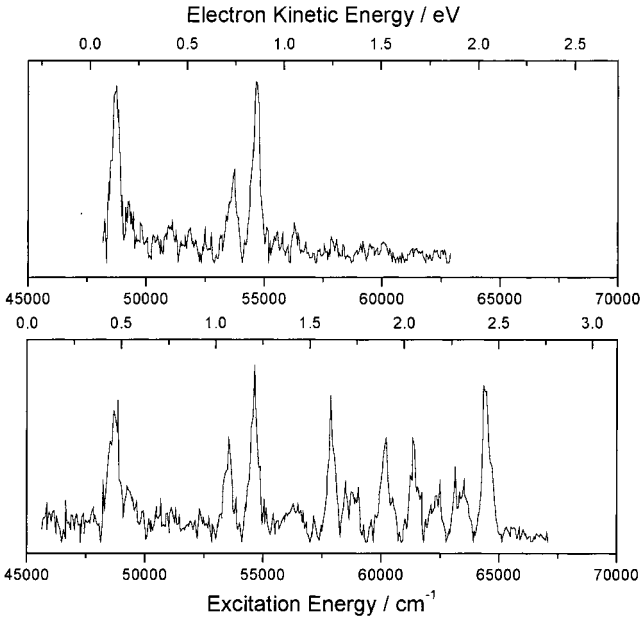

Figure 7. (3+1) REMPI photoelectron spectra of tetramethylethylene excited at 57000 cm^{-1} (top) and 65500 cm^{-1} (bottom).

state is not observed since at this excitation energy, the energy to ionize this state would need to exceed 24130 cm^{-1}. Stepwise increase of the three-photon excitation energy reveals the subsequent addition of photoelectron peaks with relatively high kinetic energies. As an example, the lower part of Figure 7 shows the photoelectron spectrum recorded at a much higher three-photon excitation energy of 65500 cm^{-1}. Once again, the photoelectron spectrum shows ionization from the Rydberg states responsible for the ionization pattern in the 57000 cm^{-1} photoelectron spectrum, but now also ionization from other, higher lying Rydberg states is observed.

The excitation energies of the Rydberg states determined in this way are given in Table 5. In general, there is good agreement between these values and the vertical excitation energies determined in previous MCD[14] and electron energy-loss (EEL)[28] studies that have been included in this Table as well. However, some discrepancies remain, the first one of which is related to the (π,3p) Rydberg manifold. Both the present study and the MCD study provide experimental evidence for two (π,3p) Rydberg states. In the MCD work they are related to features at 48909 and 51714 cm^{-1}, here we find values of 48750 and 49300 cm^{-1}. We also notice that in the EEL study just one (π,3p) Rydberg state located at 50893 cm^{-1} was reported. A possible explanation for the difference between the present and the MCD work might be that different states are observed. In that case, we must conclude that the state at 49300 cm^{-1} is a state that is not observed in MCD—that would need to be the $^1A_g(\pi,3p_x)$ state—while the state at 50893 cm^{-1} has such a low ionization probability, for example because of a large decay rate, that it does not show up in the photoelectron spectra. The EEL study reports a feature at 48635 cm^{-1} and assigns it to the $^1B_{3u}(\pi,3s) \leftarrow 1^1A_g$ transition. Our view is that this feature corresponds to the 48750 cm^{-1} transition observed here, and should consequently be reassigned to a transition to a (π,3p) Rydberg state. The MCD study assigns a feature observed between 50251 and 52632 cm^{-1} to the $^1B_{3u}(\pi,4d_\sigma)$ Rydberg state. Considering the value of the quantum defect at this energy, this cannot be true. In this energy region the EEL study reports (π,3p) and (π,3d) Rydberg states at 50893 and 52748 cm^{-1}, respectively. The present study, on the other hand, does not find any evidence for a state in this region. In the MCD study, the resonances observed at 53548 and 54315 cm^{-1} were assigned to two (π,3d) Rydberg states. We arrive at similar values (53590 and 54710 cm^{-1}), but feel that only the former feature corresponds to a (π,3d) Rydberg state whereas the other one should be associated with a (π,4s) Rydberg state. The EEL study assigns a feature at 53394 cm^{-1} as a vibrational feature of a (π,3d) Rydberg state at 52748 cm^{-1}. The presently obtained value of 53590 cm^{-1} for the excitation energy of a (π,3d) Rydberg state is very close to the value of 53394 cm^{-1}, suggesting that the latter peak should be reassigned to the origin of a (π,3d) Rydberg state.

C. Rydberg Excitations in 1,1′-Bicyclohexylidene. Up until now the only detailed investigation of the electronically excited states of BCH has been reported by Allan et al.[11] who used several spectroscopic techniques to study both the valence as well as the Rydberg states of gas-phase BCH. Although they reported the observation of several Rydberg states employing a (2+1) MPI scheme, an excitation spectrum was not depicted. Instead it was commented that "beyond a two-photon energy of 6.5 eV (52400 cm^{-1}), the MPI spectrum is intense but structureless".[11] In the context of the highly complex and congested ionization pattern of TME discussed before, this feature of the MPI spectrum of BCH can now readily be understood. Using photoelectron detection, we find in the present study that the only excited state of BCH showing a clear excitation profile is the lowest excited singlet state, the (π,3s) Rydberg state. Figure 8 shows for jet-cooled BCH its (2 + 1) excitation profile in the spectral range of 44000−46000 cm^{-1}. The ionization signal is quite weak and monitoring the signal is hindered by a relative intense (2+2) ionization signal deriving from ionization via an underlying continuum that we associate with the (π,π^*) valence state. At higher excitation energies a constant ionization signal was obtained without any indication of further resolved excited states.

Although excitation spectra can thus not provide us with the excitation energies of other Rydberg states, the intense vibronic coupling between the electronically excited states allows us to determine the excitation energies of these Rydberg states from the photoelectron spectra, similar to our approach for TME. Since BCH has a relatively high symmetry, it might be that excitation with an odd number of photons leads to the population of other states than excitation with an even number of photons. In this context one thinks in particular of the ungerade/gerade symmetry of the *anti*-conformer. We have done these experiments therefore using (2+1) as well as (3+1) ionization, but have not observed significant differences in photoelectron spectra obtained for ionization via the same intermediate energy, apart of course from the absolute values of the kinetic energies of photoelectrons.

Figure 9 shows four photoelectron spectra recorded at two-photon excitation energies of 44650, 47500, 48000, and 50000 cm^{-1}, respectively. It is clear from these spectra that increasing the excitation energy results in the appearance of additional features in the photoelectron spectra that we associate on the basis of their $\Delta v=0$ behavior in first instance with ionization from intermediate Rydberg states. As already mentioned in part A of this discussion, the photoelectron spectra do not give any indication that the *syn*- and *anti*-conformers of the molecule have different ionization properties, for example by resolvable ionization energies. We therefore will refrain from an assignment to a specific conformer, and assume that what is observed derives from both the *syn*- and the *anti*-conformer. Taking the average of peak positions associated with these ionization signals observed in several photoelectron spectra, provides us with the

TABLE 5: Summary of the Excitation Energies (cm^{-1}) and Proposed Assignments of the Rydberg States of Tetramethylethylene Obtained in the Present Study and in Previous MCD[14] and EEL[28] Studies

	present study		MCD study[14]		EEL study[28]	
assignment	energy[a]	quantum defect	assignment	energy	assignment	energy
$\pi \rightarrow 3s$	42 580	0.87	$\pi \rightarrow 3s$	42 850	$\pi \rightarrow 3s$	43 231
$\pi \rightarrow 3p_z$	48 750	0.53	$\pi \rightarrow 3p_z$	48 909		48 635[b]
$\pi \rightarrow 3p_x$	49 300	0.49			$\pi \rightarrow 3p$	50 893
			$\pi \rightarrow 3p_y$	51 714	$\pi \rightarrow 3d$	52 748
$\pi \rightarrow 3d$	53 590	0.11	$\pi \rightarrow 4d_{z^2}$	50 632−52 632	$\pi \rightarrow 3d$	53 394
$\pi \rightarrow 4s$	54 710	0.98	$\pi \rightarrow 3d_{xz}$	53 548		
$\pi \rightarrow 4p$	57 950	0.46	$\pi \rightarrow 3d_{yz}$	54 315		
$\pi \rightarrow 4p$	58 385	0.37				
$\pi \rightarrow 4d$	58 870	0.26				
$\pi \rightarrow 5s$	60 180	0.90			$\pi \rightarrow 5s$	60 007
$\pi \rightarrow 5p$	61 350	0.48				
$\pi \rightarrow 6s$	62 410	0.95				
$\pi \rightarrow 6d$	63 490	0.16			$\pi \rightarrow 6d$	63 475
$\pi \rightarrow 7s$	64 510	0.94				

[a] Values have an error margin of about ±100 cm^{-1}. [b] In the EEL study,[28] this feature has been assigned to a member of a vibrational progression associated with the (π,3s) excitation spectrum.

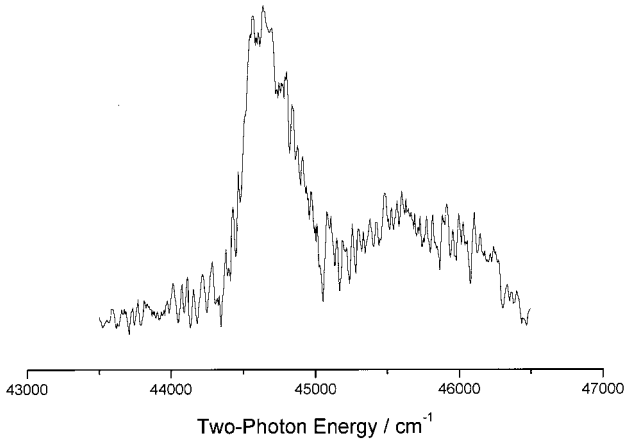

Figure 8. (2+1) REMPI excitation spectrum of jet-cooled 1,1′-bicyclohexylidene in the two-photon energy range of 44000−46000 cm^{-1}.

excitation energies of the four lower Rydberg states. These excitation energies and their assignments are reported in Table 6, together with those reported in the previous study by Allan et al.[11] In the present study we find excitation energies and associated quantum defects for the (π,3s) and the three (π,3p) Rydberg states of 44400 (0.65), 46050 (0.55), 47885 (0.41), and 48925 cm^{-1} (0.33), respectively. These values imply similar quantum defects for the (π,3p) states as compared to TME, but a significant reduction for the (π,3s) state. In view of the results of Allan et al.,[11] we wish to stress that the present study demonstrates in two independent ways the presence of a state at 44400 cm^{-1}, (i) by means of the recorded excitation spectrum, and (ii) by the photoelectron spectra described above, and photoelectron spectra to be discussed below.

The present results differ in some aspects from the previous results reported by Allan et al.[11] The most striking one is that their EEL and UV absorption studies locate the vibrationless level of the (π,3s) Rydberg state around 43500 cm^{-1} instead of 44400 cm^{-1}. Our study employing either a (1+1) or a (2+1) ionization scheme shows no evidence for a resonant feature in the excitation spectra at this energy. It might be argued that the signal we find at 44400 cm^{-1} using two-photon excitation is a vibronically induced transition of a one-photon allowed state at 43500 cm^{-1}. In that case, however, we would not expect to find in all the (2 + 1) photoelectron spectra a Rydberg-type ionization signal associated with ionization from a state apparently located at 44400 cm^{-1} but at 43500 cm^{-1}. A possible explanation for the feature observed by Allan et al.[11] is that it is a hot band transition to the (π,3s) Rydberg state that is not observed in the present study because of our use of jet-cooled expansions.

With regard to the (π,3p) Rydberg manifold, we find in the present study evidence for all three (π,3p) Rydberg states, whereas Allan et al.[11] assigned only two states. One of these states was found at 44280 cm^{-1} on the basis of the EEL spectrum (44562 cm^{-1} in MPI), but in view of our results we think that this assignment should be changed to the (π,3s) Rydberg state. The other (π,3p) Rydberg state was concluded to be located at 44957 cm^{-1} in the EEL spectrum, but we notice that the MPI and UV absorption spectra did not give evidence for a state at this energy. The value of 44957 cm^{-1} does not match with any origin determined in the present study. The closest value would be 46050 cm^{-1}, which is off by 1093 cm^{-1} and makes us suspect that the 44957 cm^{-1} feature corresponds to a vibrational transition in the (π,3s) spectrum. The previous MPI and UV absorption spectra give, on the other hand, evidence for a state around 46000 cm^{-1}, which matches excellently the value of 46050 cm^{-1} determined here.

The excitation energies of higher lying Rydberg states have been determined by recording a plethora of (2+1) and (3+1) photoelectron spectra starting from about 51000 to around 61000 cm^{-1}, close to the IP of BCH (64274 cm^{-1}),[11] and taking averages over the observed peak positions. As stated above, no fundamental difference could be observed between the ionization patterns of the two methods and we will in the following just consider the results of the (3+1) experiments. Since vibrational resolution is no longer a necessary condition for these particular experiments, the photoelectron spectra have been recorded by introducing BCH effusively at room temperature into the spectrometer. These photoelectron spectra show a complex ionization pattern corresponding to (3+1) Rydberg-type ionization from several Rydberg states, as well as weak (3+2) valence-type ionization from the underlying continuum of a valence manifold. The spectroscopic "landscape" drawn by the array of photoelectron spectra consists of four regions that display several relatively intense Rydberg-type ionization signals, which shift with the one-photon excitation energy. This is in line with our conclusion that we observe one-photon ionization from intermediate (ro)vibronic Rydberg levels populated via internal conversion from a certain vibronically excited level accessed by three-photon excitation. The four regions can roughly be divided into ionization from Rydberg states with excitation

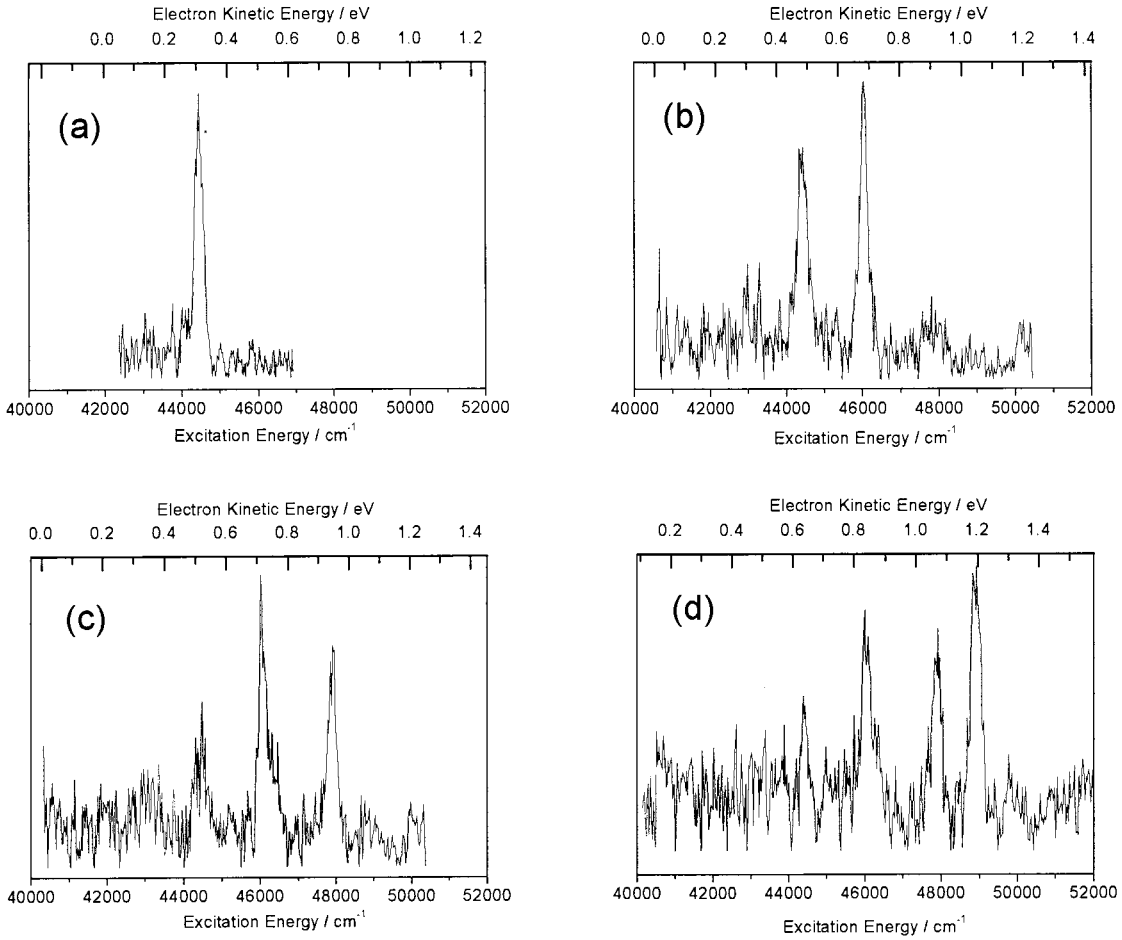

Figure 9. (2+1) REMPI photoelectron spectra of 1,1′-bicyclohexylidene excited at (a) 44650 cm^{-1}, (b) 47500, 48000, and 50000 cm^{-1}.

TABLE 6: Summary of the Excitation Energies (cm^{-1}) and Proposed Assignments of the Rydberg States of 1,1′-Bicyclohexylidene Obtained in the Present Study and in a Previous Study by Allan et al.[11]

present study REMPI-PES			Allan et al.[11] electron energy-loss spectroscopy		
assignment	energy[a]	quantum defect	assignment	energy	quantum defect
$\pi \rightarrow 3s$	44 400	0.65	$\pi \rightarrow 3s$	43 521	0.70
$\pi \rightarrow 3p$	46 050	0.55	$\pi \rightarrow 3p$	44 280	0.66
$\pi \rightarrow 3p$	47 885	0.41	$\pi \rightarrow 3p$	44 957	0.62
$\pi \rightarrow 3p$	48 925	0.33			
$\pi \rightarrow 3d$	51 175	0.11			
$\pi \rightarrow 3d$	51 775	0.04	$\pi \rightarrow 3d$	51 700	0.05
$\pi \rightarrow 3d$	52 375	0.00			
$\pi \rightarrow 4s$	54 770	0.60	$\pi \rightarrow 4s$	53 797	0.76
$\pi \rightarrow 4p$	55 320	0.50			
$\pi \rightarrow 4p$	55 710	0.42			
$\pi \rightarrow 4p/4d$	56 510	0.24			
$\pi \rightarrow 4d$	57 255	0.05			
$\pi \rightarrow 5s$	57 940	0.84			
$\pi \rightarrow 5p$	59 115	0.39			
$\pi \rightarrow 5d$	59 750	0.07	$\pi \rightarrow 5d$	59 765	0.07
$\pi \rightarrow 6p$	60 833	0.35			

[a] Values have an error margin of about ± 100 cm^{-1}.

energies located in the (i) 44000−49000 cm^{-1}, (ii) 51000−53000 cm^{-1}, (iii) 54000−57000 cm^{-1}, and (iv) 58000−61000 cm^{-1} regions. Ionization from the 44000−49000 cm^{-1} region is relatively weak and sometimes even not observable because of the fact that the three-photon excitation energy may not always be sufficient to ionize the molecule from the Rydberg states in this region.

Figure 10 shows (3+1) photoelectron spectra that are representative for the other three regions. The upper photoelectron spectrum taken at 52100 cm^{-1} shows two peaks at higher kinetic energies that can be associated with ionization from excited states located around 52100 and 51800 cm^{-1}. Assignment in terms of Rydberg states would lead, on the basis of the quantum defects, to an assignment as two 3d Rydberg states. The low-energy features correspond to ionization from vibrationally excited levels of Rydberg states with excitation energies of 48729 and 47737 cm^{-1}, respectively. These values are in good agreement with those obtained from the (2+1) photoelectron spectra of Figure 9 for two of the (π,3p) Rydberg states. Increasing the three-photon excitation energy to 56600 cm^{-1} (middle part of Figure 10) leads, apart from the ionization signals already observed in the previous photoelectron spectrum recorded at 52100 cm^{-1}, to the appearance of several other intense ionization signals around 1.2−1.4 eV. Three intense features can be observed at 1.365, 1.269, and 1.219 eV. A fourth, weaker feature is located at 1.155 eV. The three intense ionization features correspond to ionization from vibronic levels of states with excitation energies and quantum defects of 56414 (0.26), 55640 (0.43), and 55237 cm^{-1} (0.52), respectively. On the basis of these quantum defects, one readily assigns the latter two states as (π,4p) Rydberg states, but the first state might either be a (π,4p) or a (π,4d) Rydberg state. The weak feature at 1.155 eV corresponds to ionization from a vibrationally excited level of a state with an excitation energy of 54721 cm^{-1} that might be assigned as the (π,4s) or (π,4p) Rydberg state. Assignment as a (π,4p) state would imply that the state at 56414 cm^{-1} should be assigned as a (π,4d) state, but would also mean

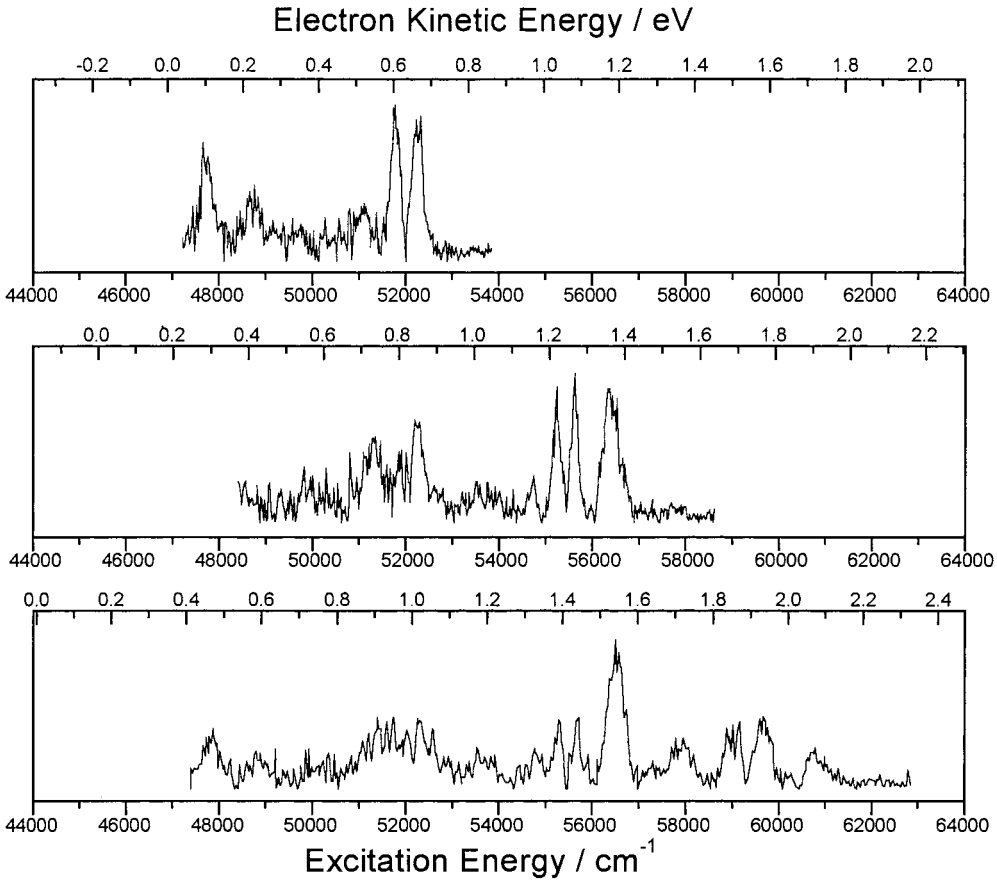

Figure 10. (3+1) REMPI photoelectron spectra of 1,1′-bicyclohexylidene excited at 52100 cm^{-1} (top), 56600 cm^{-1} (middle), and 60600 cm^{-1} (bottom).

that we observe the $n=3$ and $n=5$ members of the ns Rydberg series, and not the $n=4$ member. Assignment as the (π,4s) state, on the other hand, would imply a quantum defect of 0.61 for this state. Considering that the (π,5s) state has a much larger quantum defect of 0.85 (vide infra), and that for TME considerably larger values of the quantum defect are found for the ns Rydberg states, forces us to put the assignment of this state as a pure Rydberg state into question. In fact, even the assignment of the state at 44400 cm^{-1} as a pure (π,3s) Rydberg state might on the basis of the quantum defect of 0.65 be considered debatable.

The lower photoelectron spectrum in Figure 10 shows that the increase of the three-photon excitation energy to 60600 cm^{-1} results in the addition of four more, relatively fast, ionization signals that we associate with ionization from the (π,6p), (π,5d), (π,5p), and (π,5s) states at around 60600, 59600, 59000, and 58000 cm^{-1}. A complete survey of all the states observed in the present study in this way is listed in Table 6. Also given in this table are the excitation energies and assignments for the Rydberg states observed by Allan et al.[11] They have reported three features beyond 51000 cm^{-1}, namely, at 51700, 53797, and 59765 cm^{-1}, which they assigned to a (π,3d), the (π,4s), and a (π,5d) Rydberg state, respectively. The values reported for the (π,3d) and the (π,5d) Rydberg state are in excellent agreement with our values. The excitation energy of their (π,4s) state is − similar to what was observed for the (π,3s) state − again about 1000 cm^{-1} higher than observed in our studies.

D. Valence Excitations in Tetramethylethylene and 1,1′-Bicyclohexylidene. In excited-state photoelectron spectroscopy an intermediate electronically excited state is characterized by projecting its (ro)vibronic wave function onto the ground state of the lowest radical cation D_0. Rydberg states with potential energy surfaces resembling closely that of D_0 may therefore be expected to show up prominently due to relatively large Franck−Condon factors. Valence states, on the other hand, have a potential energy surface that generally is different from that of D_0, and thus smaller Franck−Condon factors associated with them in the ionization process. This holds in particular for the (π,π^*) valence state of mono-olefins having a perpendicular equilibrium geometry. Although the electronic oscillator strength associated with valence states is typically 10−100 times larger than that of the lower Rydberg states, their highly unfavorable vibrational overlap with the vibrational manifold of D_0 may thus result in an overall resonance-enhanced multiphoton ionization cross section that is significantly larger for Rydberg states than for valence states. An ab initio study by Mebel et al.,[39] in which the low-energy region of the excitation profile of the lower Rydberg states and the (π,π^*) valence state was simulated, has shown this aspect quite convincingly for ethylene. Here we find a similar situation for the role of the (π,π^*) valence state in TME and BCH: a continuous background signal is observed from this state that reflects one- and two-photoionization to all available vibrational levels in the ionic state. The highly complex and congested nature of the ionization pattern for BCH, as well as that for TME, is remarkable since a recent excited-state photoelectron spectroscopic study on jet-cooled ethylene[34] did not reveal any experimental evidence of vibronic coupling between the lowest Rydberg states and the underlying continuum of the (π,π^*) valence state. This leads to the idea that the intense vibronic coupling in BCH and TME between the Rydberg and valence manifold is a consequence of the dramatic increase in the density of states for these two mono-olefinic compounds as compared to their parent molecule ethylene.

One of the goals of the present study was to investigate the nature of the—presumed valence—state around 55000 cm^{-1} in BCH. As outlined in the Introduction, several suggestions have been put forward for the assignment of this state $-\sigma \rightarrow \sigma^*$; $\pi \rightarrow \sigma^*$; $\pi(CH_2) \rightarrow \pi^* -$, but all of them imply a different potential energy surface as compared to a Rydberg state. The idea was therefore that around these excitation energies a different ionization pattern should be observed in the photoelectron spectra that could give us clues on the characteristics of this state. Photoelectron spectra obtained with two- and three-photon excitation, however, do not give any indication that at these excitation energies something fundamentally different is happening in the photoionization process: the continuous valence background associated with one- and two-photon ionization is present in the same way as at lower excitation energies, and all one observes is ionization from apparent Rydberg-type states. This suggests not only that the previous assignments in terms of excitation from an occupied valence orbital to an unoccupied valence orbital might be questioned but also that one would need to come up with a scenario in which this second valence-like state behaves in the ionization process as a Rydberg state.

One possible and rather attractive explanation is based upon Rydberg-valence mixing as has been discussed extensively by Peyerimhoff and others for ethylene.[23,70] In ethylene the (π,π^*) and (π,$3d_{xz}$) states have the same radial and angular nodal structure, and mixing between both states can be anticipated. Because of this mixing, the two states obtain different properties: the (π,π^*) state becomes more like a Rydberg state—losing oscillator strength and becoming electronically more diffuse—whereas the (π,$3d_{xz}$) state will become more like a valence state—gaining oscillator strength and becoming electronically more compact. Ab initio studies on ethylene have by now reached consensus that mixing between the (π,π^*) valence state and the (π,$3d_{xz}$) Rydberg state is in fact quite small.[71−74] It is important to notice, however, that an increased mixing may be expected when the energy gap between these two excited states decreases. Since the excitation energy of a Rydberg state is related to the ionization energy via the Rydberg formula, and since the value of the ionization energy is dropping fast upon alkylation of the C=C bond,[23] the excitation energy of the (π,3d) Rydberg manifold is significantly lower for BCH and TME than for ethylene. Bearing in mind that alkylation of the C=C bond has a smaller effect on the excitation energy of the (π,π^*) valence state,[23] the energy gap between the (π,π^*) valence state and the (π,3d) Rydberg manifold is expected to be smaller in BCH and TME than in ethylene, and thus Rydberg-valence mixing to be increased in the former compounds. A recent ab initio study on the excited states of a wide range of alkylated mono-olefins ranging from propylene to BCH[75] has provided support for such an enhancement of Rydberg-valence coupling, and shows evidence for strong Rydberg-valence mixing in TME and BCH.

This coupling between the (π,π^*) valence state and the (π,3d) Rydberg manifold should of course not only be restricted to BCH, but be valid for all mono-olefins containing an isolated C=C bond, although its influence depends on the structural properties of the mono-olefin and on the number of alkyl side groups attached to its C=C bond. Clark et al.[10] have compared their UV absorption spectrum of BCH vapor with that of a number of similar compounds and concluded that the two intense absorption bands at 48000 and 55000 cm^{-1} in the UV absorption spectrum of BCH occur in all mono-olefins, but that in many instances they are approximately degenerate. Experimental evidence for the presence of not just one—the (π,π^*) valence state—but two low-lying excitations in mono-olefins with considerable oscillator strength has come from several spectroscopic studies.[13,24,76] First, if one compares the absorption spectrum of TME vapor at 298 K with that of a thin film of TME at 23 K,[24] a pronounced shoulder shows up in the solid-state spectrum around 50000 cm^{-1}. Second, the VUV absorption spectrum of propylene[76] shows two intense broad bands associated with valence-like excitations: one around 58000 cm^{-1} assigned to the (π,π^*) state, and a second one close to 69000 cm^{-1} that has been assigned previously to a $\sigma \rightarrow \sigma^*$ transition involving the C−H of the methyl group. A final example involves the results of a polarization study of electronic transitions in the steroids Δ^4- and Δ^5-cholestene.[13] In this study it was concluded that olefins having symmetrically substituted C=C bonds show two absorption bands of similar intensity, both of which are polarized along their C=C bond. The absorption spectrum of Δ^4- and Δ^5-cholestene shows two intense broad absorption features with maxima around 49400 and 52600 cm^{-1}, which is very similar to the absorption maxima of the two low-lying valence-like excitations in BCH.

The above scenario accounts for the Rydberg-like ionization behavior of this second valence-like state. Which state that would be in the photoelectron spectra is less clear. Above we have indicated for BCH that there are some states that seem to have irregular quantum defects, and also in the case of TME one can in retrospect claim that there are states with a peculiar quantum defect, e.g., the 4d Rydberg state, but it is clear that this is too weak a basis for an unambiguous assignment. Measurements of photoelectron angular distributions would in this respect be most useful to distinguish the various states. A final point is that it would be attractive to be able to distinguish between the *syn*- and *anti*-conformations of BCH. Study of the separately accessible *syn*- and *anti*-forms of 4,4′-di-*tert*-butylbicyclohexylidene[61] is anticipated to provide insight into the importance of these conformational aspects. Such studies will shortly be initiated.

The present experiments and considerations apply to the gas phase. One might therefore wonder how intermolecular interactions as they occur in solution or in the solid-state affect the present picture. The energy difference between the (π,π^*) state and the interacting Rydberg state is in that discussion an important parameter. Although Rydberg states are rather susceptible to external perturbations, external perturbations are not expected to affect their excitation energy to such an extent that their interaction with the valence state is changed significantly. We therefore expect that the present picture will also hold under nonisolated conditions.

IV. Conclusions

The olefins TME and BCH have been investigated employing multiphoton excitation in combination with excited-state photoelectron spectroscopy. Although excitation spectra have turned out to be only of limited use to obtain excitation energies of excited states in these molecules—resonance enhancement rapidly disappears—excited-state photoelectron spectroscopy has proven to be highly efficient to probe the Rydberg manifold over the full spectral range of both mono-olefins, and to determine the excitation energies of a plethora of excited states. The reason for this effectiveness is that the photophysics of TME as well as BCH are heavily dominated by vibronic coupling within the full manifold of the excited singlet states, or considered in the time domain, by highly efficient internal conversion.

The photoelectron spectra obtained for BCH have shown that the state that in previous work was assigned as a second valence

state does not give the clear signature one might expect on the basis of the hypotheses made for its electronic character. In contrast, all that is observed are Rydberg-type ionization patterns with an underlying quasi-continuum assigned to ionization from the (π,π*) valence state. This has led us to consider the present results in the light of the Rydberg-valence mixing in the parent compound ethylene. On that basis an explanation has been put forward that involves extensive mixing between the (π,π*) valence state and the Rydberg manifold. It has been shown that it offers an attractive explanation as well for the observation of two low-lying valence-like excitations for other mono-olefinic compounds. Such a mixing will be substantiated in a forthcoming publication in which the spectroscopic properties of excited states of alkyl-substituted mono-olefenic compounds have been investigated with ab initio calculations.[75]

Acknowledgment. The authors would like to thank Ing. D. Bebelaar for valuable technical support, and Prof. Dr. C. A. de Lange and Prof. Dr. M. Glasbeek for use of equipment.

References and Notes

(1) Lehn, J.-M. *Angew. Chem., Int Ed. Engl.* **1990**, *29*, 1304.
(2) Whitesides, G. M.; Mathias, J. P.; Seto, C. T. *Science* **1991**, *254*, 1312.
(3) Wong, M. S.; Bosshard, C.; Günther, P. *Adv. Mater.* **1997**, *9*, 837.
(4) Metzger, R. M. *J. Mater. Chem.* **1999**, *9*, 2027.
(5) Hoogesteeger, F. J.; van Walree, C. A.; Jenneskens, L. W.; Roest, M. R.; Verhoeven, J. W.; Schuddeboom, W.; Piet, J. J.; Warman, J. M. *Chem. Eur. J.* **2000**, *6*, 2948.
(6) Oosterbaan, W. D.; Havenith, R. W. A.; van Walree, C. A.; Jenneskens, L. W.; Gleiter, R.; Kooijman, H.; Spek, A. L. *J. Chem. Soc., Perkin Trans. 2* **2001**, 1066.
(7) Bakkers, E. P. A. M.; Roest, A. L.; Marsman, A. W.; Jenneskens, L. W.; de Jong-van Steensel, L. I.; Kelly, J. J.; Vanmaekelbergh, D. *J. Phys. Chem. B* **2000**, *104*, 7266.
(8) Bakkers, E. P. A. M.; Marsman, A. W.; Jenneskens, L. W.; Vanmaekelbergh, D. *Angew. Chem. Int. Ed.* **2000**, *39*, 2297.
(9) Marsman, A. W.; Leussink, E. D.; Zwikker, J. W.; Jenneskens, L. W.; Smeets, W. J. J.; Veldman, N.; Spek, A. L. *Chem. Mater.* **1999**, *11*, 1484.
(10) Snyder, P. A.; Clark, L. B. *J. Chem. Phys.* **1970**, *52*, 998.
(11) Allan, M.; Snyder, P. A.; Robin, M. B. *J. Phys. Chem.* **1985**, *89*, 4900.
(12) Hoogesteeger, F. J.; Havenith, R. W. A.; Zwikker, J. W.; Jenneskens, L. W.; Kooijman, H.; Veldman, N.; Spek, A. L. *J. Org. Chem.* **1995**, *60*, 4375.
(13) Yogev, A.; Sagiv, J.; Mazur, Y. *J. Am. Chem. Soc.* **1972**, *94*, 5122.
(14) Snyder, P. A.; Hansen, R. W. C.; Rowe, E. M. *J. Phys. Chem.* **1996**, *100*, 17756.
(15) Watson Jr., F. H.; Nycum, M. W. *Spectrosc. Lett.* **1975**, *8*, 223.
(16) Hoogesteeger, F. J.; van Lenthe, J. H.; Jenneskens, L. W. *Chem. Phys. Lett.* **1996**, *259*, 178.
(17) Petrongolo, C.; Buenker, R. J.; Peyerimhoff, S. D. *J. Chem. Phys.* **1982**, 76, 3655.
(18) Peyerimhoff, S. D.; Buenker, R. J. *Theor. Chim. Acta* **1972**, *27*, 243.
(19) Petrongolo, C.; Buenker, R. J.; Peyerimhoff, S. D. *J. Chem. Phys.* **1983**, 78, 7284.
(20) Havenith, R. W. A.; van Lenthe, J. H.; Jenneskens, L. W.; Hoogesteeger, F. J. *Chem. Phys.* **1997**, *225*, 139.
(21) Havenith, R. W. A.; van Dam, H. J. J.; van Lenthe, J. H.; Jenneskens, L. W. *Chem. Phys.* **1999**, *246*, 49.
(22) Havenith, R. W. A.; Jenneskens, L. W.; van Lenthe, J. H. *Chem. Phys. Lett.* **1998**, *282*, 39.
(23) Robin, M. B. *Higher Excited States of Polyatomic Molecules*; Academic Press: New York, 1985; Vol. III.
(24) Robin, M. B.; Hart, R. R.; Kuebler, N. A. *J. Chem. Phys.* **1966**, *44*, 1803.
(25) Siebrand, W.; Dedonder-Lardeux, C.; Jouvet, C. *Chem. Phys. Lett.* **1990**, *174*, 559.
(26) Hirayama, F.; Lipsky, S. *J. Chem. Phys.* **1975**, *62*, 576.
(27) Inoue, Y.; Daino, Y.; Hakushi, T.; Okada, T. *J. Am. Chem. Soc.* **1989**, *111*, 5584.
(28) Johnson, K. E.; Johnston, D. B.; Lipsky, S. *J. Chem. Phys.* **1979**, *70*, 3844.
(29) Wickramaaratchi, M. A.; Preses, J. M.; Weston, R. E., Jr. *Chem. Phys. Lett.* **1985**, *120*, 491.
(30) Watson Jr., F. H.; Armstrong, A. T.; McGlynn, S. P. *Theor. Chim. Acta* **1970**, *16*, 75.
(31) Watson Jr., F. H.; McGlynn, S. P. *Theor. Chim. Acta* **1971**, *21*, 309.
(32) Evans, D. F. *Proc. R. Soc., London* **1963**, 378.
(33) Langford, S. R.; Orr-Ewing, A. J.; Morgan, R. A.; Western, C. M.; Ashfold, M. N. R.; Rijkenberg, R. A.; Scheper, C. R.; Buma, W. J.; de Lange, C. A. *J. Chem. Phys.* **1998**, *108*, 6667.
(34) Rijkenberg, R. A.; Buma, W. J., *J. Phys. Chem. A* **2002**, *106*, 3727.
(35) Wiberg, K. B.; Hadad, C. M.; Foresman, J. B.; Chupka, W. A. *J. Phys. Chem.* **1992**, *96*, 10756.
(36) McMurchie, L. E.; Davidson, E. R. *J. Chem. Phys.* **1977**, *67*, 5613.
(37) Foresman, J. B.; Head-Gordon, M.; Pople, J. A.; Frisch, M. J. *J. Phys. Chem.* **1992**, *96*, 135.
(38) Mebel, A. M.; Chen, Y.-T.; Lin, S. H. *Chem. Phys. Lett.* **1996**, *258*, 53.
(39) Mebel, A. M.; Chen, Y.-T.; Lin, S. H. *J. Chem. Phys.* **1996**, *105*, 9007.
(40) Rijs, A. M.; Backus, E. H. G.; de Lange, C. A.; Westwood, N. P. C.; Janssen, M. H. M. *J. Electron Spectrosc. Relat. Phenom.* **2000**, *112*, 151.
(41) Scheper, C. R.; Buma, W. J.; de Lange, C. A. *J. Electron Spectrosc. Relat. Phenom.* **1998**, *97*, 147.
(42) Kruit, P.; Read, F. H. *J. Phys. E* **1983**, *16*, 313.
(43) Köppel, H.; Domcke, W.; Cederbaum, L. S.; von Niessen, W. *J. Chem. Phys.* **1978**, *69*, 4252.
(44) Pollard, J. E.; Trevor, D. J.; Reutt, J. E.; Lee, Y. T.; Shirley, D. A. *J. Chem. Phys.* **1984**, *81*, 5302.
(45) Wang, L.; Pollard, J. E.; Lee, Y. T.; Shirley, D. A. *J. Chem. Phys.* **1987**, *86*, 3216.
(46) Buenker, R. J.; Peyerimhoff, S. D.; Hsu, H. L. *Chem. Phys. Lett.* **1971**, *11*, 65.
(47) Veldman, N.; Spek, L. A.; Hoogesteeger, F. J.; Zwikker, J. W.; Jenneskens, L. W. *Acta Crystallogr. C* **1994**, *50*, 742.
(48) Asveld, E. W. H.; Kellog, R. M. *J. Org. Chem.* **1982**, *47*, 1250.
(49) Takahashi, O.; Kikuchi, O. *J. Mol. Struct. (THEOCHEM)* **1994**, *313*, 207.
(50) Merer, A. J.; Schoonveld, L. *Can. J. Phys.* **1969**, *47*, 1731.
(51) Gedanken, A.; Kuebler, N. A.; Robin, M. B. *J. Chem. Phys.* **1982**, *76*, 46.
(52) Williams, B. A.; Cool, T. A. *J. Chem. Phys.* **1991**, *94*, 6358.
(53) Mintz, D. M.; Kuppermann, A. *J. Chem. Phys.* **1979**, *71*, 3499.
(54) Rauhut, G.; Pulay, P. *J. Phys. Chem.* **1995**, *99*, 3093.
(55) Scott, A. P.; Radom, L. *J. Phys. Chem.* **1996**, *100*, 16502.
(56) Durig, J. R.; Hawley, C. W. *J. Chem. Phys.* **1972**, *57*, 1426.
(57) Scott, D. W.; Waddington, G.; Smith, J. C.; Huffman, H. M. *J. Am. Chem. Soc.* **1949**, *71*, 2767.
(58) Scott, D. W.; Flinke, H. L.; McCullough, J. P.; Gross, M. E.; Messerly, J. F.; Pennington, R. E.; Waddington, G. *J. Am. Chem. Soc.* **1955**, *77*, 4993.
(59) Handschuh, P.; Nagel, B.; Fruwert, J. *Z. Chem.* **1984**, *24*, 199.
(60) Nagel, B.; Handschuh, P.; Fruwert, J.; Geiseler, G. *Z. Phys. Chem.* **1984**, *265*, 474.
(61) Marsman, A. W.; Havenith, R. W. A.; Bethke, S.; Jenneskens, L. W.; Gleiter, R.; van Lenthe, J. H.; Lutz, M.; Spek, A. L. *J. Org. Chem.* **2000**, *65*, 4584.
(62) Siebrand, W.; Zerbetto, F.; Zgierski, M. Z. *Chem. Phys. Lett.* **1990**, *174*, 119.
(63) Masclet, P.; Grosjean, D.; Mouvier, G. *J. Electron Spectrosc. Relat. Phenom.* **1973**, *2*, 225.
(64) McDiarmid, R. *J. Chem. Phys.* **1969**, *50*, 2328.
(65) Chau, F. T. *J. Mol. Struct.* **1985**, *131*, 383.
(66) Spangler, L. H.; Bosma, W. B.; van Zee, R. D.; Zwier, T. S. *J. Chem. Phys.* **1988**, *88*, 6768.
(67) Yan, S.; Spangler, L. H. *J. Phys. Chem.* **1995**, *99*, 3047.
(68) Siewert, S.; Spangler, L. H. *J. Phys. Chem.* **1995**, *99*, 9316.
(69) Metzger, B. S.; Spangler, L. H. *J. Phys. Chem. A* **1997**, *101*, 5431.
(70) Buenker, R.; Peyerimhoff, S. D. *Chem. Phys. Lett.* **1975**, *36*, 415.
(71) Krebs, S.; Buenker, R. J. *J. Chem. Phys.* **1997**, *106*, 7208.
(72) Buenker, R. J.; Shih, S.-K.; Peyerimhoff, S. D. *Chem. Phys.* **1979**, *36*, 97.
(73) Müller, T.; Dallos, M.; Lischka, H. *J. Chem. Phys.* **1999**, *110*, 7176.
(74) Wiberg, K. B.; Hadad, C. M.; Foresman, J. B.; Chupka, W. A. *J. Phys. Chem.* **1992**, *96*, 10756.
(75) Rijkenberg, R. A.; Buma, W. J.; van Walree, C. A.; Jenneskens, L. W.; Schmal, L. P.; van Lenthe, J. H. Manuscript in preparation.
(76) Iverson, A. A.; Russel, B. R.; Jones, P. R. *Chem. Phys. Lett.* **1972**, *17*, 98.